Improved chloride quantification in quadrupole aerosol chemical speciation monitors (Q-ACSMs)

Anna K. Tobler[1], Alicja Skiba[2], Dongyu S. Wang[1], Philip Croteau[3], Katarzyna Styszko[4], Jarosław Nęcki[2],
5 Urs Baltensperger[1], Jay G. Slowik[1] and André S. H. Prévôt[1]

[1]Laboratory of Atmospheric Chemistry, Paul Scherrer Institute, 5232 Villigen PSI, Switzerland
[2] AGH University of Science and Technology, Faculty of Physics and Applied Computer Science, Department of Applied
Nuclear Physics, 30-059 Krakow, Poland
[3]Aerodyne Research, Inc, Billerica, Massachusetts, USA
10 [4]AGH University of Science and Technology, Faculty of Energy and Fuels, Department of Coal Chemistry and Environmental
Sciences, 30-059 Krakow, Poland

Correspondence to: Jay G. Slowik (jay.slowik@psi.ch) and André S.H. Prévôt (andre.prevot@psi.ch)

Abstract. Particulate chloride is an important component of fine particulate matter in marine air masses. Recent field studies
15 also report elevated concentrations of gas-phase reactive chlorine species and particulate chloride related to anthropogenic
activities. This work focuses on particulate chloride detection and quantification issues observed for some quadrupole aerosol
chemical speciation monitors (Q-ACSM), which are designed for long-term measurement of ambient aerosol composition.
The ACSM reports particle concentrations based on the difference between measurements of ambient air (sample mode) and
particle-free ambient air (filter mode). For our long-term campaign in Krakow, Poland, the Q-ACSM reports apparent negative
20 total chloride concentration for most of the campaign when analyzed with the default fragmentation table. This is the result of
the difference signal from m/z 35 ($^{35}Cl^+$) being negative which dominates over the positive difference signal from m/z 36
($H^{35}Cl^+$). Highly time-resolved experiments with NH_4Cl, $NaCl$ and KCl particles show that the signal response of m/z 35 is
non-ideal, where the signal builds up and decreases slowly for all three salts, leading to a negative difference measurement. In
contrast, the m/z 36 signal exhibits a near step-change response for NH_4Cl during sampling and filter period, resulting in a
25 positive difference signal. The response of m/z 36 for $NaCl$ and KCl is not as prompt as for NH_4Cl but still fast enough to have
a positive difference signal. Furthermore, it is shown that this behavior is mostly temperature-independent. Based on these
observations, this work presents an approach to correct the chloride concentration time series by adapting the standard
fragmentation table coupled with a calibration of NH_4Cl to obtain a relative ionization efficiency (RIE) based on the signal at
m/z 36 ($H^{35}Cl^+$). This correction can be applied for measurements in environments where chloride is dominated by NH_4Cl.
30 Caution should be exercised when other chloride salts dominate the ambient aerosol.

1   Introduction

Aerosols are known to have a significant influence on regional to global climate and visibility (Fuzzi et al., 2015). Furthermore, severe adverse health effects have been linked to aerosol exposure (Pope and Dockery, 2006). Therefore, a better understanding of the aerosol composition is crucial. In recent years, different types of Aerodyne aerosol mass spectrometers (AMS (Jayne et al., 2000)) and aerosol chemical speciation monitors (ACSM (Ng et al., 2011)) have been widely used to quantify the chemical composition of non-refractory (NR) particulate matter (PM) with high time resolution. They allow simultaneous quantification of NR-PM chloride, ammonium, nitrate, organics and sulfate. For many environments, chloride does not significantly contribute to the total mass (Jimenez et al., 2009). Exceptions include coastal regions influenced by marine aerosol masses which are rich in inorganic sea salt (Ovadnevaite et al., 2012) and polluted inland regions influenced by anthropogenic chloride emissions. Anthropogenic chloride emissions include HCl which then forms NH_4Cl with ammonia (NH_3). Particulate chloride can enable heterogeneous production of $ClNO_2$ via reactive uptake of N_2O_5 during nighttime, which photolyzes to produce highly reactive chlorine radicals in the daytime (Yang et al., 2018; Le Breton et al., 2018). The chlorine radical undergoes hydrogen-abstraction reactions with hydrocarbons to form HCl which then again forms NH_4Cl (Chang and Allen, 2006). This can lead to exceptionally high chloride concentrations as has been reported for New Delhi by Gani et al. (2019) and Tobler et al. (2020).

ACSMs equipped with a quadrupole mass spectrometer (Q-ACSM, (Ng et al., 2011)) have been used in numerous field campaigns in various environments. The first ambient intercomparison of 13 individual Q-ACSMs, carried out in the vicinity of Paris, revealed good correlation between the Q-ACSMs for all species except chloride. It was not clear if this was due to low concentrations near the detection limit or due to the non-ideal vaporization behavior of chloride, which depends on the specific conditions in the individual instruments (Crenn et al., 2015). During our long-term (> 1 year) measurement campaign in Krakow, Poland, we observed significant apparent negative chloride concentrations, especially during the winter season when aerosol concentrations are high in general. The fragmentation table (Allan et al., 2004) attributes each m/z to one or more of the bulk species, i.e. nitrate, ammonium, sulfate, organics and chloride. By default, the chloride concentration is calculated based on the measured $^{35}Cl^+$ (m/z 35) and $H^{35}Cl^+$ (m/z 36) ion signals and the estimated $^{37}Cl^+$ (m/z 37) and $H^{37}Cl^+$ (m/z 38) ion signals, calculated based on the natural isotope ratio of chlorine (see Table 1). Measurements with negative signal from either m/z 35 or 36 can therefore result in total negative chloride concentrations. The behavior of some chloride salts in the AMS has been studied. For example Ovadnevaite et al. (2012) demonstrated that sea salt can be quantified by an AMS despite the mostly refractory nature of NaCl. Drewnick et al. (2015) showed that chloride salts appear to be sticky on the vaporizer surface and are only slowly removed. Also, chloride can undergo chemical reactions with the tungsten vaporizer surface resulting in WO_2Cl_2, among other compounds. Furthermore, they showed that chloride detection suffers from vaporizer memory effects, as demonstrated by the presence of several iron chloride signals when iron nitrate nonahydrate was injected after chloride experiments. For the Q-ACSM, detection and quantification issues for organic chloride have been reported for isoprene-

derived secondary organic aerosol (Wang and Hildebrandt Ruiz, 2017). To our knowledge, there are no studies focused on the response of Q-ACSM to inorganic chlorides.

65 In this study, we are able to attribute the issue of reported negative chloride concentrations in Q-ACSMs to a negative difference signal at m/z 35. We present a highly time-resolved characterization of the Q-ACSM response to three different chloride salts at different vaporizer temperatures. Finally, we propose a calibration procedure coupled with a change in the fragmentation table to improve chloride detection and quantification using the Q-ACSM.

2   Method

70 The operating principle of the ACSM is described in detail by Ng et al. (2011) and is briefly summarized here. The ACSM alternatively samples directly from ambient air ("sample") and through a particle filter ("filter"), switching every 30 s. After passing through a 100 μm critical orifice, the submicron particles are focused into a narrow beam by an aerodynamic lens. Non-refractory particles are flash-vaporized upon impact with the standard tungsten vaporizer at ~600 °C, where it is assumed that the solid particle is quickly turned into a vapor without undergoing any other processes besides thermal decomposition.

75 For the ACSM used in this study (SN 140-145), an yttriated iridium filament was used to ionize the resulting vapors via electron impact (EI). The ions are detected by a quadrupole residual gas analyzer (RGA, Pfeiffer Vacuum Prisma Plus). The difference of the sample and the filter measurements represents the aerosol mass spectrum. The obtained mass spectrum typically ranges between m/z 10 and 150 with unit mass resolution (UMR).

Investigations with different high-purity chloride salts were performed. Ammonium chloride (NH_4Cl), sodium chloride (NaCl)
80 and potassium chloride (KCl) were separately dissolved in ultrapure water. Mono-disperse particles with a diameter of 300 nm were generated using a Topas atomizer, a krypton source as a bipolar charger and a custom-made differential mobility analyzer (DMA). The particles were simultaneously injected into the ACSM and a condensation particle counter (CPC, TSI model 3022A). The standard vaporizer voltage was set to 7.7 V, corresponding to a vaporizer temperature of 720 °C, throughout the full campaign and was not changed unless otherwise mentioned. Calibrations were performed with the same
85 setup using aqueous solutions of ammonium nitrate (NH_4NO_3), ammonium sulfate (($NH_4)_2SO_4$) and ammonium chloride (NH_4Cl), following the new recommended calibration procedure, which measures in full scan mode, meaning that the same scanning protocol as during ambient measurements is used during the calibration (Freney et al., 2019).

The presented ambient online measurements were conducted at the AGH University of Science and Technology in Krakow, Poland (50°04' N, 19°55' E) between 8 January 2018 and 10 April 2019. The inlet was installed 2 m above the rooftop of the
90 building and was equipped with a 5 L min^{-1} PM$_{2.5}$ cyclone (BGI, Mesa Labs, Inc.). The aerosol was dried through a Nafion dryer in the temperature-controlled room before being sampled by the ACSM. The data was recorded with a resolution of 10 min unless specified otherwise. All data were analyzed using ACSM Local 1.6.1.3 (Aerodyne Research Inc.) in Igor 6.37 (Wavemetrics Inc.).

Atmospheric
Measurement
Techniques
Discussions

3   Results and discussion

3.1   Observations in ambient measurements

The Q-ACSM was installed at AGH University in Krakow for > 14 months. The time series of chloride and the other NR-PM species are shown in Fig. 1a and 1b. During the first month of the measurements, significant positive chloride concentrations were measured. However, shortly after, the contribution of chloride decreased and, from the end of February 2018 until the end of the campaign, apparent negative chloride concentrations were recorded.

The chloride concentration is calculated based on the m/z 35 ($^{35}Cl^+$), m/z 36 ($H^{35}Cl^+$), m/z 37 ($^{37}Cl^+$), and m/z 38 ($H^{37}Cl^+$) signals (Table 1). The $^{35}Cl^+$ and $H^{35}Cl^+$ are measured, whereas the $^{37}Cl^+$ and $H^{37}Cl^+$ signals are calculated based on the natural isotopic ratio of ^{35}Cl to ^{37}Cl and therefore will not be discussed further. While the signal of m/z 36 is positive throughout the full campaign (Fig. 1c), the signal of m/z 35 turns negative in February 2018 (Fig. 1d), which results in an apparent negative concentration of the total chloride signal (Fig. 1b). Similar observations of apparent negative chloride concentrations have been seen in Măgurele, Romania, during long-term field measurements (L. Marmureanu, personal communication).

Under typical operating conditions, the Q-ACSM scans the mass range from m/z 10–150 at a scan rate of 200 ms amu^{-1}, which produces a full mass spectrum roughly every 30 s. To better understand the transient behavior of m/z 35 and m/z 36, only those two ions were scanned with high time resolution, leading to a signal with 1 s resolution. To simulate the typical ambient ACSM sample/filter switching, the filter was switched every 30 s. Results shown in Fig. 2 explain how the different response times of Cl$^+$ and HCl$^+$ result in the apparent negative chloride: While HCl$^+$ behaves nearly ideally and the signal instantaneously reacts after the filter change, Cl$^+$ slowly builds up or slowly decays in the 30 s following a filter change. During normal full-spectra scans, the ions are subsequently measured in the quadrupole, meaning that the Cl$^+$ and HCl$^+$ signals used to calculate the difference signal are measured approximately 5 s after the filter switch, as indicated by the markers in Fig. 2. Consequently, the difference signal (i.e. "sample" – "filter") for m/z 36 is positive, whereas the difference signal for m/z 35 is negative under normal operating conditions.

3.2   Behavior of selected chloride salts in the Q-ACSM

The behaviors of the slowly vaporizing Cl$^+$ and the rapidly vaporizing HCl$^+$ of three of the most abundant chloride salts in the atmosphere were studied in more detail using NH$_4$Cl, NaCl and KCl. Similarly to the highly time-resolved targeted m/z measurements for the ambient sample, only m/z 35 and m/z 36 were monitored on a 1 s resolution basis with filter switching every 30 s.

In Fig. 3 the averaged temporal development of the signal in sample and filter mode for each of the three chloride salts is shown. The signals for NaCl and KCl are normalized to the signal of NH$_4$Cl. There are apparent differences between NH$_4$Cl and the other two salts, as well as between the m/z's. The signal for NH$_4$Cl responds faster after the filter switching, particularly for m/z 36 where a prompt increase and decrease of the signal after the filter switch can be observed. In contrast, the signal of NaCl and KCl evolves much more slowly. This different response time between the salts is also observed for m/z 35, however

to a much smaller extent. The observation of the m/z 36 (HCl$^+$) signal for NaCl and KCl, even though their direct thermal composition products do not include HCl(g), is probably the result of heat-induced chemical reactions between chloride and background water vapor (Drewnick et al., 2015).

In addition, the behavior of the different chloride salts at different vaporizer voltages (i.e. temperatures) was studied. The relative temporal evolution is mostly independent of the vaporizer temperature for all three salts investigated. The temporal behavior of the signal of NH$_4$Cl is shown in Fig. 4. Similar to the usual vaporizer temperature of this instrument (7.7 V), the signal at m/z 35 evolves much more slowly than the signal at m/z 36 at all temperatures. Near identical temporal trends are observed for the signal at m/z 36 for vaporizer voltages below 7.7 V. Above this voltage, a jump in the ion baseline intensity is observed. For the signal m/z 35 a similar trend is visible, however, the differences between the signals for vaporizer voltages $\leq$ 7.7 V are larger. For NaCl and KCl a similar trend is observed (Fig. S1 and S2), where the background signal for NaCl is already starting to build up at 7.7 V. The signal of the background is a combination of several processes that can be expected to be enhanced or suppressed by the higher temperature, including increased flash vaporization of chloride at vaporizer surface, suppressed condensation at/near the vaporizer surface, enhanced re-desorption at/near vaporizer surface, and condensation and re-desorption near the filament. To which extent each of these processes contribute to the jump in the instrument background cannot be decoupled based on the available measurements.

In the AMS (and therefore also in the ACSM), NH$_4$Cl is expected to undergo thermal decomposition via the reaction NH$_4$Cl(s) → NH$_3$(g) + HCl(g) ((Hu et al., 2017) and references therein). This flash-vaporizing dissociation pathway results in signal at m/z 36 from HCl$^+$. However, it is also possible that the particles can remain on the vaporizer or bounce off the vaporizer and land on a nearby, cooler surface, e.g., on the ionization chamber walls, and vaporize at a slower rate. During this process, further chemical reaction may occur, e.g. the vaporizer surface can act as catalyst for reactions with other aerosol components or material on the vaporizer or the vaporizer material itself. For instance, production of different tungsten oxide chlorides are reported for a porous tungsten vaporizer (standard vaporizer) (Drewnick et al., 2015). Regardless of the reactions, any of these multi-step processes would be much more likely to suppress the m/z 36 signal and enhance the m/z 35 signal. For example, it can be expected that tungsten oxide chlorides, produced by reaction with the vaporizer, will result in a Cl$^+$ signal rather than an HCl$^+$ signal.

The quantification of ACSM (and AMS) data relies on the imperfect assumption that all measured particles flash-vaporize on the initial impact with the vaporizer. However, the behavior of some compounds such as ammonium sulfate and certain organic molecules can deviate from that of an ideal non-refractory component (Huffman et al., 2005). The behavior of semi-refractory compounds can strongly depend on the instrument history, vaporizer temperature, instrument tuning, filament material, and the physical alignment of the filament and is therefore hard to predict. The temperature in the ionization chamber is influenced by the vaporizer temperature itself, the filament temperature, and the alignment of those to each other. Nowadays, ACSMs are equipped with tungsten filaments. However, older ACSMs were delivered with yttriated iridium filaments, which is also the case for the ACSM used here for all measurements. There are no direct measurements available to compare the temperature of the ion source between these two systems. However, based on the material properties, the iridium filament is expected to

Atmospheric
Measurement
Techniques
Discussions

160   have a lower temperature compared to the tungsten filaments and therefore the iridium filament is expected to have more slow-vaporizing components compared to the tungsten filament. For example, apparent negative chloride concentrations were reported for the Romanian ACSM mentioned earlier when operated with an iridium filament. After changing to a tungsten filament, the total chloride concentration was positive (L. Marmureanu, personal communication). Based on the observations, it is also possible that the capture vaporizer (Hu et al., 2017; Xu et al., 2017) can increase the possibility of negative m/z 35,

165   as there is more collision of HCl(g) with the hot vaporizer surface which could result in more m/z 35 signal.

Regardless of how consistent the effect is between different Q-ACSMs, the fact that a difference between m/z 35 and m/z 36 regarding the vaporization times can be observed, suggests that the m/z 35 signal should be utilized with caution even when negative difference signals are not detected. Analogous to Ovadnevaite et al. (2012), where the NaCl$^+$ ion was suggested as a surrogate for sea salt due to its more rapid evaporation, here we recommend to use the HCl$^+$ ion as the signature for NH$_4$Cl, as

170   it is the direct product of thermal decomposition and less influenced by secondary, lower-temperature vaporization. It also leads to more consistent results over time as the time-response of Cl$^+$ at m/z 35 is hard to predict as described above.

3.3   Corrections

The chloride calculation is based on the frag_chloride entry in the fragmentation table (Allan et al., 2004), which is actually a combination of frag_Cl and frag_HCl (Table 1, in black). Our experimental results suggest that the Cl$^+$ signal originates from

175   slow thermal decomposition of NH$_4$Cl and biases the calculation of the total chloride concentration. HCl, the thermal decomposition product of NH$_4$Cl, also fragments into Cl$^+$, however, this is calculated based on the HCl$^+$ signal. Therefore, the Cl$^+$ signal from frag_Cl should not be used in the calculation and we suggest to adapt the fragmentation table by multiplying the frag_Cl by zero (Table 1, in red). Similar suggestions were made for the quantification of organochlorides (Wang and Hildebrandt Ruiz, 2017).

180   As described by (Ng et al., 2011), the mass concentration C_s of the species s is calculated from the ion signals I at its mass spectral fragments i, taking into account the molar weight MW_s and the ionization efficiency (IE) of the species, the volumetric sample flow Q_v, Avogadro's number N_A and a conversion factor of 10^{12}:

$$C_s = \frac{10^{12} \cdot MW_s}{IE_s \cdot Q \cdot N_A} \sum_{all\ i} I_{s,i} \tag{1}$$

The slower detection electronics of a Q-ACSM do not allow a direct measurement of the IE, but the response factor (RF) of

185   the instrument is related to the IE through Avogadro's number N_A, the molar mass MW, the flow Q_{cal} and the electron multiplier gain G_{cal}:

$$IE_{NO_3} \cdot \frac{N_A}{MW_{NO_3}} = \frac{RF_{NO_3}}{Q_{cal} \cdot G_{cal}} \tag{2}$$

Instead of determining the IE_s for each species, it is more convenient to express the IE$_s$ relative to the IE of NO$_3$ (IE$_{NO3}$) as the so-called relative ionization efficiency (RIE$_s$) for each species.

190
$$\frac{IE_s}{MW_s} = RIE_s \cdot \frac{IE_{NO_3}}{MW_{NO_3}}$$
(3)

Routinely, the ACSM is calibrated with NH_4NO_3 and $(NH_4)_2SO_4$ to determine the RF_{NO3}, RIE_{NH4} and RIE_{SO4}. Whereas the RF_{NO3} is based on m/z 30 and 46, the RIE_{NH4} and RIE_{SO4} are based on all ion signals of the species. In order to quantify the chloride mass properly, the ACSM is also calibrated with NH_4Cl to determine the RIE_Chl'. While the standard RIE_{Chl} is based on all ion signals for chloride assigned in the standard fragmentation table, we firstly adapted the fragmentation table as

195   described above for the calculation of the RIE_Chl', meaning that the RIE_Chl' is only based on the ion signals of frag_HCl and does not include frag_Cl. Details on the calculation of the RIEs can be found in the supplement section S1. Five calibrations over the course of 7 months (October 2018 – April 2019) resulted in an average RIE_Chl' = 0.41 ± 0.17, $RIE_{NH4} = 2.43 \pm 0.58$ and $RIE_{SO4} = 0.38 \pm 0.11$ with $RF_{NO3} = 4.68 \pm 1.66 \cdot 10^{-11}$ amps (µg m^{-3})$^{-1}$. In general, the calibrated RIE values are lower than the default values commonly used in the ACSM. Notably, the RIE_Chl' is significantly lower than the default value of 1.3.

200   The ACSM is recommended to be routinely calibrated not only with NH_4NO_3 but also with $(NH_4)_2SO_4$, because it has been shown that the RIE_{SO4} value can be quite different from the default value of 1.2 (Budisulistiorini et al., 2014; Crenn et al., 2015; Freney et al., 2019), as it is also the case for this instrument.

The relation of m/z 36 to the total chloride mass depends strongly on the chloride salt present, as discussed in Section 3.2. NH_4Cl exhibits a prompt signal response at m/z 36, whereas the NaCl and KCl signals build up more slowly. It still results in

205   a slightly positive difference signal for those two chloride salts. However, the ratio of m/z 36 to the total chloride mass will be different. Therefore, in the absence of a single dominant cation, quantification should be treated with care due to the effect of the salt-dependent vaporization kinetics on the m/z 36 difference signal.

Comparison of the highly time-resolved chloride salt calibrations with ambient measurements, as well as the correlation of m/z 36 with NH_4^+ ($R^2 = 0.58$), m/z 23 (Na^+, $R^2 = 0.37$) and m/z 39 (K^+, $R^2 = 0.13$, though possibly influenced by $C_3H_3^+$ ions) suggest

210   that NH_4Cl was likely the dominant fine chloride species in the ambient aerosol in Krakow, Poland. The correlation of m/z 36 and m/z 58 (potentially $NaCl^+$, $R^2 = 0.71$) and m/z 74 (potentially KCl^+, $R^2 = 0.79$) is high, though this is likely the result of correlation of m/z 36 with total organics ($R^2 = 0.60$), which could produce ions at the same nominal m/z (e.g. $C_3H_6O^+$, $C_2H_2O_2^+$ and $C_4H_{10}^+$ at m/z 58, and $C_6H_2^+$, $C_3H_6O_2^+$ and $C_4H_{10}O^+$ at m/z 74), which cannot be separated from metal halide ions with UMR data. Therefore, application of the above described correction of the fragmentation table and calibration should yield

215   accurate quantification of chloride. Fig. 5 shows the corrected chloride time series.

Time-of-flight instruments like the ToF-ACSM (Fröhlich et al., 2013) and ToF-AMS (Drewnick et al., 2005; DeCarlo et al., 2006) typically do not suffer from negative m/z 35 signal, even though similar vaporizer and ionizer configurations are used, due to the different measurement technique of the detector (no scanning over the full mass range). However, one would expect to measure roughly 0 at m/z 35 since the average value of the sample rise and the filter decay are about equal. Therefore, the

220   calculation methodology presented here can provide more accurate/repeatable quantification regardless of the instrument.

4   Conclusions

Apparent negative chloride concentrations were measured during a long-term campaign in Krakow, Poland resulting from slow vaporization of NH_4Cl at m/z 35, when using the standard ACSM fragmentation table. Highly time-resolved measurements of different chloride salts confirm a different behavior of $^{35}Cl^+$ (m/z 35) and $H^{35}Cl^+$ (m/z 36). m/z 36 shows a
225 prompt signal response, whereas m/z 35 responds more slowly which may lead to a negative difference signal for that ion. The extent to which this happens can strongly depend on instrument history, tuning and alignment in the ionizer cage and is hard to predict. Even when an instrument is not apparently affected by negative m/z 35 signal, one should consider using the revised fragmentation table presented here for chloride along with an instrument specific RIE_Chl' so that the total chloride mass is calculated only based on the m/z 36 signal.

230 Q-ACSM users should consider modifying the fragmentation table and, when doing so, include NH_4Cl in routine calibrations throughout the campaign. The RIE_Chl' value of 0.41 presented here should be considered as a guidance and is only valid for this particular instrument. We suggest that routine calibration with NH_4Cl be utilized to determine this value for a particular instrument when better quantification of chloride is desired. Future ACSM intercomparisons will provide an opportunity to study this issue in more detail.

235

References

255   Allan, J. D., Delia, A. E., Coe, H., Bower, K. N., Alfarra, M. R., Jimenez, J. L., Middlebrook, A. M., Drewnick, F., Onasch, T. B., Canagaratna, M. R., Jayne, J. T., and Worsnop, D. R.: A generalised method for the extraction of chemically resolved mass spectra from aerodyne aerosol mass spectrometer data, J. Aerosol Sci., 35, 909-922, https://doi.org/10.1016/j.jaerosci.2004.02.007, 2004.

Budisulistiorini, S. H., Canagaratna, M. R., Croteau, P. L., Baumann, K., Edgerton, E. S., Kollman, M. S., Ng, N. L., Verma,
260   V., Shaw, S. L., Knipping, E. M., Worsnop, D. R., Jayne, J. T., Weber, R. J., and Surratt, J. D.: Intercomparison of an Aerosol Chemical Speciation Monitor (ACSM) with ambient fine aerosol measurements in downtown Atlanta, Georgia, Atmos. Meas. Tech., 7, 1929-1941, https://doi.org/10.5194/amt-7-1929-2014, 2014.

Chang, S., and Allen, D. T.: Chlorine chemistry in urban atmospheres: Aerosol formation associated with anthropogenic chlorine emissions in southeast Texas, Atmos. Environ., 40, 512-523, https://doi.org/10.1016/j.atmosenv.2006.04.070, 2006.

265   Crenn, V., Sciare, J., Croteau, P. L., Verlhac, S., Frohlich, R., Belis, C. A., Aas, W., Auml;ijala, M., Alastuey, A., Artinano, B., Baisnee, D., Bonnaire, N., Bressi, M., Canagaratna, M., Canonaco, F., Carbone, C., Cavalli, F., Coz, E., Cubison, M. J., Esser-Gietl, J. K., Green, D. C., Gros, V., Heikkinen, L., Herrmann, H., Lunder, C., Minguillon, M. C., Mocnik, G., O'Dowd, C. D., Ovadnevaite, J., Petit, J. E., Petralia, E., Poulain, L., Priestman, M., Riffault, V., Ripoll, A., Sarda-Esteve, R., Slowik, J. G., Setyan, A., Wiedensohler, A., Baltensperger, U., Prevot, A. S. H., Jayne, J. T., and Favez, O.: ACTRIS
270   ACSM intercomparison - Part 1: Reproducibility of concentration and fragment results from 13 individual Quadrupole Aerosol Chemical Speciation Monitors (Q-ACSM) and consistency with co-located instruments, Atmos. Meas. Tech., 8, 5063-5087, https://doi.org/10.5194/amt-8-5063-2015, 2015.

DeCarlo, P. F., Kimmel, J. R., Trimborn, A., Northway, M. J., Jayne, J. T., Aiken, A. C., Gonin, M., Fuhrer, K., Horvath, T., Docherty, K. S., Worsnop, D. R., and Jimenez, J. L.: Field-deployable, high-resolution, time-of-flight aerosol mass
275   spectrometer, Anal. Chem., 78, 8281-8289, https://doi.org/10.1021/ac061249n, 2006.

Drewnick, F., Hings, S. S., DeCarlo, P., Jayne, J. T., Gonin, M., Fuhrer, K., Weimer, S., Jimenez, J. L., Demerjian, K. L., Borrmann, S., and Worsnop, D. R.: A new time-of-flight aerosol mass spectrometer (TOF-AMS) - Instrument description and first field deployment, Aerosol Sci. Tech., 39, 637-658, https://doi.org/10.1080/02786820500182040, 2005.

Drewnick, F., Diesch, J. M., Faber, P., and Borrmann, S.: Aerosol mass spectrometry: particle-vaporizer interactions and
280   their consequences for the measurements, Atmos. Meas. Tech., 8, 3811-3830, https://doi.org/10.5194/amt-8-3811-2015, 2015.

Freney, E., Zhang, Y. J., Croteau, P., Amodeo, T., Williams, L., Truong, F., Petit, J. E., Sciare, J., Sarda-Esteve, R., Bonnaire, N., Arumae, T., Aurela, M., Bougiatioti, A., Mihalopoulos, N., Coz, E., Artinano, B., Crenn, V., Elste, T., Heikkinen, L., Poulain, L., Wiedensohler, A., Herrmann, H., Priestman, M., Alastuey, A., Stavroulas, I., Tobler, A.,
285   Vasilescu, J., Zanca, N., Canagaratna, M., Carbone, C., Flentje, H., Green, D., Maasikmets, M., Marmureanu, L., Minguillon, M. C., Prevot, A. S. H., Gros, V., Jayne, J., and Favez, O.: The second ACTRIS inter-comparison (2016) for Aerosol Chemical Speciation Monitors (ACSM): Calibration protocols and instrument performance evaluations, Aerosol Sci. Tech., https://doi.org/10.1080/02786826.2019.1608901, 2019.

Fröhlich, R., Cubison, M. J., Slowik, J. G., Bukowiecki, N., Prevot, A. S. H., Baltensperger, U., Schneider, J., Kimmel, J. R.,
290   Gonin, M., Rohner, U., Worsnop, D. R., and Jayne, J. T.: The ToF-ACSM: a portable aerosol chemical speciation monitor with TOFMS detection, Atmos. Meas. Tech., 6, 3225-3241, https://doi.org/10.5194/amt-6-3225-2013, 2013.

Fuzzi, S., Baltensperger, U., Carslaw, K., Decesari, S., van Der Gon, H. D., Facchini, M. C., Fowler, D., Koren, I., Langford, B., Lohmann, U., Nemitz, E., Pandis, S., Riipinen, I., Rudich, Y., Schaap, M., Slowik, J. G., Spracklen, D. V., Vignati, E.,

Wild, M., Williams, M., and Gilardoni, S.: Particulate matter, air quality and climate: lessons learned and future needs,
295   Atmos. Chem. Phys., 15, 8217-8299, https://doi.org/10.5194/acp-15-8217-2015, 2015.

Gani, S., Bhandari, S., Seraj, S., Wang, D. S., Patel, K., Soni, P., Arub, Z., Habib, G., Hildebrandt Ruiz, L., and Apte, J.:
Submicron aerosol composition in the world's most polluted megacity: the Delhi Aerosol Supersite study, Atmos. Chem.
Phys., 19, 6843-6859, https://doi.org/10.5194/acp-19-6843-2019, 2019.

Hu, W. W., Campuzano-Jost, P., Day, D. A., Croteau, P., Canagaratna, M. R., Jayne, J. T., Worsnop, D. R., and Jimenez, J.
300   L.: Evaluation of the new capture vapourizer for aerosol mass spectrometers (AMS) through laboratory studies of inorganic
species, Atmos. Meas. Tech., 10, 2897-2921, https://doi.org/10.5194/amt-10-2897-2017, 2017.

Huffman, J. A., Jayne, J. T., Drewnick, F., Aiken, A. C., Onasch, T., Worsnop, D. R., and Jimenez, J. L.: Design, modeling,
optimization, and experimental tests of a particle beam width probe for the aerodyne aerosol mass spectrometer, Aerosol Sci.
Tech., 39, 1143-1163, https://doi.org/10.1080/02786820500423782, 2005.

305   Jayne, J. T., Leard, D. C., Zhang, X. F., Davidovits, P., Smith, K. A., Kolb, C. E., and Worsnop, D. R.: Development of an
aerosol mass spectrometer for size and composition analysis of submicron particles, Aerosol Sci. Tech., 33, 49-70,
https://doi.org/10.1080/027868200410840, 2000.

Jimenez, J. L., Canagaratna, M. R., Donahue, N. M., Prevot, A. S., Zhang, Q., Kroll, J. H., DeCarlo, P. F., Allan, J. D., Coe,
H., Ng, N. L., Aiken, A. C., Docherty, K. S., Ulbrich, I. M., Grieshop, A. P., Robinson, A. L., Duplissy, J., Smith, J. D.,
310   Wilson, K. R., Lanz, V. A., Hueglin, C., Sun, Y. L., Tian, J., Laaksonen, A., Raatikainen, T., Rautiainen, J., Vaattovaara, P.,
Ehn, M., Kulmala, M., Tomlinson, J. M., Collins, D. R., Cubison, M. J., Dunlea, E. J., Huffman, J. A., Onasch, T. B.,
Alfarra, M. R., Williams, P. I., Bower, K., Kondo, Y., Schneider, J., Drewnick, F., Borrmann, S., Weimer, S., Demerjian, K.,
Salcedo, D., Cottrell, L., Griffin, R., Takami, A., Miyoshi, T., Hatakeyama, S., Shimono, A., Sun, J. Y., Zhang, Y. M.,
Dzepina, K., Kimmel, J. R., Sueper, D., Jayne, J. T., Herndon, S. C., Trimborn, A. M., Williams, L. R., Wood, E. C.,
315   Middlebrook, A. M., Kolb, C. E., Baltensperger, U., and Worsnop, D. R.: Evolution of organic aerosols in the atmosphere,
Science, 326, 1525-1529, https://doi.org/10.1126/science.1180353, 2009.

Le Breton, M., Hallquist, Å. M., Pathak, R. K., Simpson, D., Wang, Y., Johansson, J., Zheng, J., Yang, Y., Shang, D., Wang,
H., Liu, Q., Chan, C., Wang, T., Bannan, T. J., Priestley, M., Percival, C. J., Shallcross, D. E., Lu, K., Guo, S., Hu, M., and
Hallquist, M.: Chlorine oxidation of VOCs at a semi-rural site in Beijing: significant chlorine liberation from ClNO2 and
320   subsequent gas- and particle-phase Cl–VOC production, Atmos. Chem. Phys., 18, 13013-13030, https://doi.org/10.5194/acp-
18-13013-2018, 2018.

Ng, N. L., Herndon, S. C., Trimborn, A., Canagaratna, M. R., Croteau, P. L., Onasch, T. B., Sueper, D., Worsnop, D. R.,
Zhang, Q., Sun, Y. L., and Jayne, J. T.: An Aerosol Chemical Speciation Monitor (ACSM) for routine monitoring of the
composition and mass concentrations of ambient aerosol, Aerosol Sci. Tech., 45, 780-794,
325   https://doi.org/10.1080/02786826.2011.560211, 2011.

Ovadnevaite, J., Ceburnis, D., Canagaratna, M., Berresheim, H., Bialek, J., Martucci, G., Worsnop, D. R., and O'Dowd, C.:
On the effect of wind speed on submicron sea salt mass concentrations and source fluxes, J. Geophys. Res.-Atmos., 117,
https://doi.org/10.1029/2011jd017379, 2012.

Pope, C. A., and Dockery, D. W.: Health effects of fine particulate air pollution: Lines that connect, J. Air Waste Manage.,
330   56, 709-742, https://doi.org/10.1080/10473289.2006.10464485, 2006.

Tobler, A., Bhattu, D., Canonaco, F., Lalchandani, V., Shukla, A., Thamban, N., Mishra, S., Tiwari, S., Mocnik, G.,
Baltensperger, U., Tripathi, S. N., Slowik, J. G., and Prévôt , A. S. H.: Chemical characterization of PM2.5 and source
apportionment of organic aerosol in New Delhi, India, Submitted to Sci. Total Environ., 2020.

Wang, D. Y. S., and Hildebrandt Ruiz, L.: Secondary organic aerosol from chlorine-initiated oxidation of isoprene, Atmos.
335   Chem. Phys., 17, 13491-13508, https://doi.org/10.5194/acp-17-13491-2017, 2017.

Xu, W., Croteau, P., Williams, L., Canagaratna, M., Onasch, T., Cross, E., Zhang, X., Robinson, W., Worsnop, D., and
Jayne, J.: Laboratory characterization of an aerosol chemical speciation monitor with PM2.5 measurement capability,
Aerosol Sci. Tech., 51, 69-83, https://doi.org/10.1080/02786826.2016.1241859, 2017.

Yang, X., Wang, T., Xia, M., Gao, X., Li, Q., Zhang, N., Gao, Y., Lee, S., Wang, X., Xue, L., Yang, L., and Wang, W.:
340   Abundance and origin of fine particulate chloride in continental China, Sci. Total Environ., 624, 1041-1051,
https://doi.org/10.1016/j.scitotenv.2017.12.205, 2018.

Atmospheric
Measurement
Techniques

Open Access

Discussions

EGU

345 **Table 1. The original fragmentation table (black) is a combination of the frag_Cl and frag_HCl. Because of the non-ideal behavior of *m/z* 35, it is recommended to adapt (red) the fragmentation table for chloride, so that it is only based on frag_HCl.**

m/z	frag_chloride	frag_Cl	frag_HCl
35	frag_HCl[35],**0***frag_Cl[35]	35,-frag_HCl[35]	0.231*frag_HCl[36]
36	frag_HCl[36]		36,-frag_air[36]
37	frag_HCl[37],**0***frag_Cl[37]	0.323*frag_Cl[35]	0.323*frag_HCl[35]
38	frag_HCl[38]		0.323*frag_HCl[36]

Figure 1. (a) Stacked time series of NH₄, NO₃, Org and SO₄ and (b) time series of chloride in µg m⁻³. Panels (c) and (d) show the time series of *m/z* 35 and *m/z* 36 in amps, respectively. The negative chloride signal is driven by the negative *m/z* 35 signal.
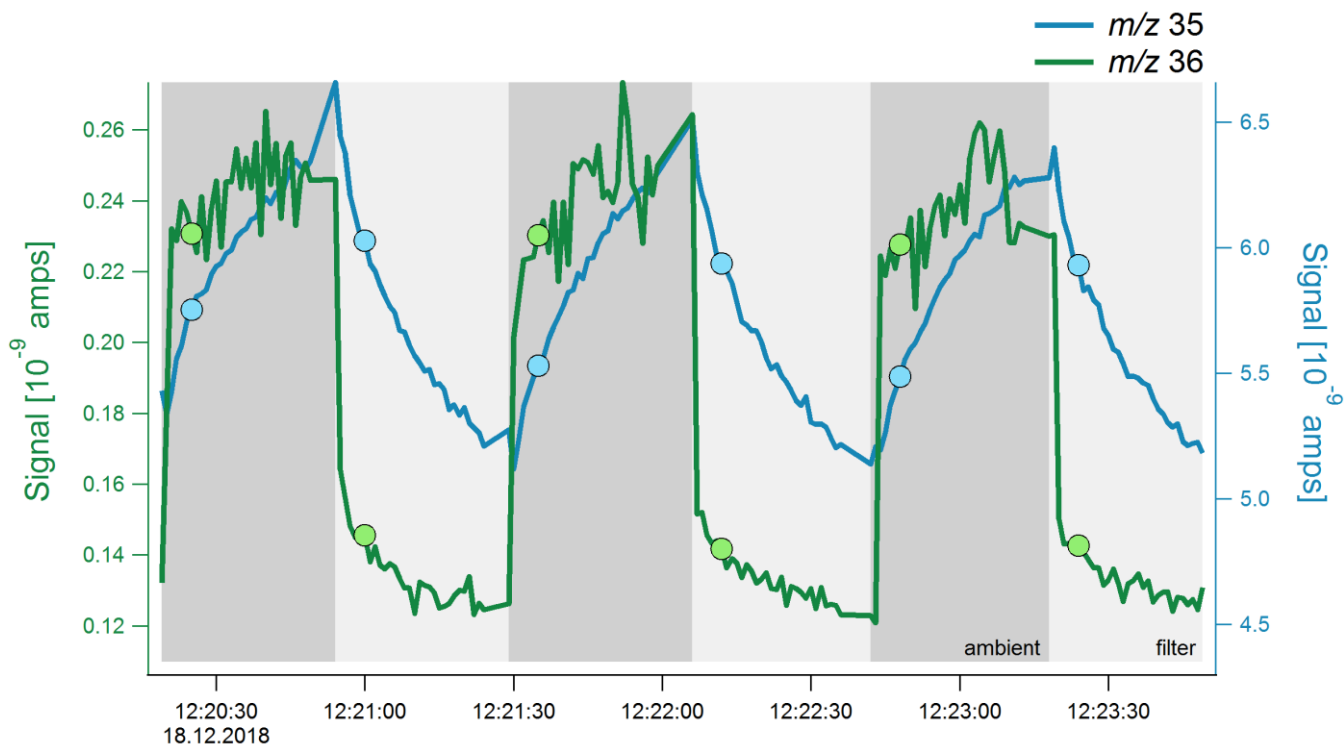
350

Figure 2. High–resolution time series (1 Hz) of the total ambient signal at *m/z* 35 (blue) and *m/z* 36 (green) signal. The filter was switched every 30 s to simulate normal measurements, the filter and ambient mode are indicated by the different shades of grey. The dots mark the time at which these *m/z*'s are scanned in the quadrupole during normal measurements, which is typically around 5 s after the filter switch.
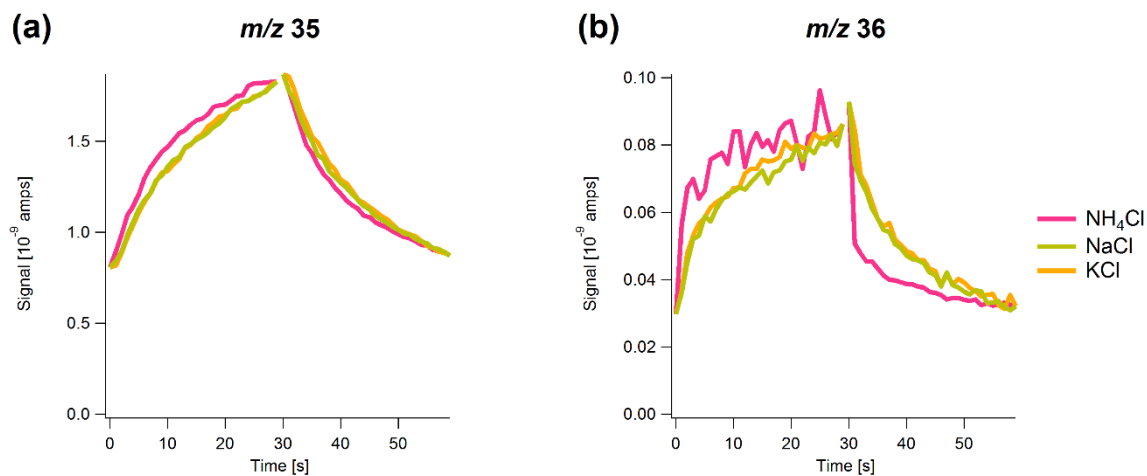
Figure 3. Time series of the signal of (a) *m/z* 35 and (b) *m/z* 36 with 1 s resolution over a simulated sample/filter cycle for NH₄Cl (pink), NaCl (green) and KCl (orange). The signal of NaCl and KCl are normalized to the one of NH₄Cl.
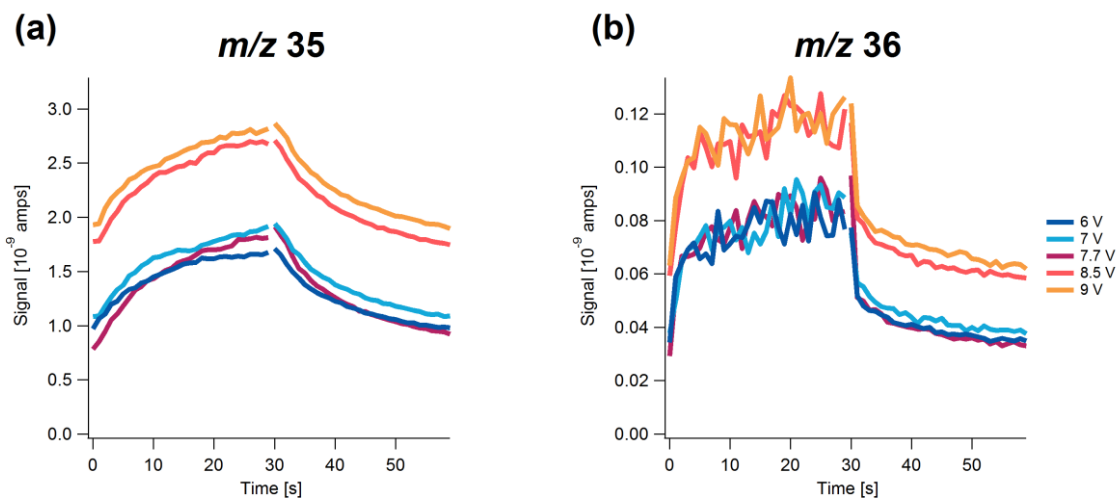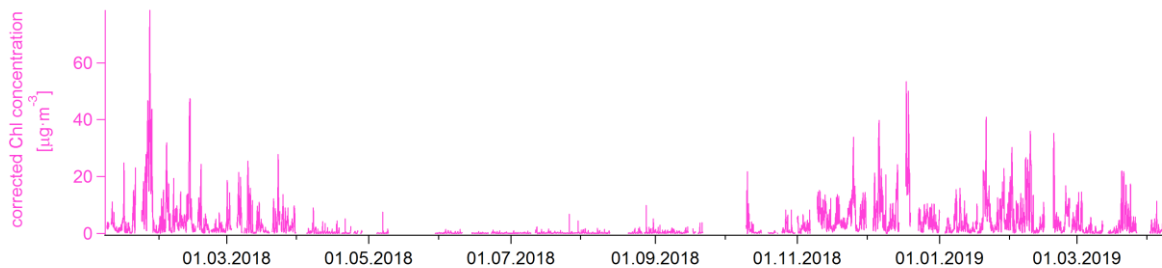
360

Figure 4. Highly time-resolved signal of (a) *m/z 35* **and (b)** *m/z 36* **as a function of time at different vaporizer voltages (i.e. temperatures) over a simulated sample/filter cycle for NH₄Cl.**

Figure 5. Time series of chloride after recalculation based on fragmentation table adjustments and RIE_Chl' derived from NH₄Cl calibration.